

1 **Monitoring high-ozone events in the US Intermountain West using TEMPO**
2 **geostationary satellite observations**

3

4 Peter Zoogman^{1, †, *}, Daniel J. Jacob^{1,2}, Kelly Chance³, Xiong Liu³, Meiyun Lin⁴, Arlene Fiore⁵,
5 Katherine Travis²

6

7 1 Department of Earth and Planetary Sciences, Harvard University, Cambridge, MA, United
8 States

9 2 School of Engineering and Applied Sciences, Harvard University, Cambridge, MA, United
10 States

11 3 Harvard-Smithsonian Center for Astrophysics, Cambridge, MA, United States

12 4 Atmospheric and Ocean Sciences, Princeton University, Princeton, New Jersey, USA

13 5 Lamont-Doherty Earth Observatory, Columbia University, Palisades, NY, United States

14 † Present Address: Harvard-Smithsonian Center for Astrophysics, Cambridge, MA, United
15 States

16 *Corresponding Author. Tel: 9176129834. E-mail: pzoogman@cfa.harvard.edu. 60 Garden
17 Street, Cambridge, MA 02138

18 **Abstract**

19 High-ozone events, approaching or exceeding the National Ambient Air Quality Standard
20 (NAAQS), are frequently observed in the US Intermountain West in association with subsiding
21 air from the free troposphere. Monitoring and attribution of these events is problematic because
22 of the sparsity of the current network of surface measurements and lack of vertical information.
23 We present an Observing System Simulation Experiment (OSSE) to evaluate the ability of the
24 future geostationary satellite instrument Tropospheric Emissions: Monitoring of Pollution
25 (TEMPO), scheduled for launch in 2018-2019, to monitor and attribute high-ozone events in the
26 Intermountain West through data assimilation. TEMPO will observe ozone in the ultraviolet
27 (UV) and visible (Vis) to provide sensitivity in the lower troposphere. Our OSSE uses ozone data
28 from the GFDL AM3 chemistry-climate model (CCM) as the “true” atmosphere and samples it
29 for April-June 2010 with the current surface network (CASTNet sites), TEMPO, and a low Earth
30 orbit (LEO) IR satellite instrument. These synthetic data are then assimilated into the GEOS-
31 Chem chemical transport model (CTM) using a Kalman filter. Error correlation length scales
32 (500 km in horizontal, 1.7 km in vertical) extend the range of influence of observations. We
33 show that assimilation of surface data alone does not adequately detect high-ozone events in the
34 Intermountain West. Assimilation of TEMPO data greatly improves the monitoring capability,
35 with little information added from the LEO instrument. The vertical information from TEMPO
36 further enables the attribution of NAAQS exceedances to background ozone. This is illustrated
37 with the case of a stratospheric intrusion.

38

39 **1. Introduction**

40 Harmful impacts of surface level ozone on both humans and vegetation is of increasing
41 concern in areas formerly considered remote. The US Environmental Protection Agency (EPA) is
42 considering lowering the current National Ambient Air Quality Standard (NAAQS) of 75 ppbv (fourth
43 highest maximum daily 8-hour average per year) to a value in the range of 60-70 ppbv (EPA, 2012).
44 Ozone concentrations in this range are frequently observed at high-elevation sites in the western US
45 with minimal local pollution influence (Lefohn et al., 2001). Although ozone levels have been
46 decreasing over the eastern US for the past two decades due to emissions controls, there has been no
47 such decrease in the West except for California (Cooper et al., 2012). Free tropospheric ozone at
48 3-8 km altitude over the western US has been increasing by 0.41 ppbv year⁻¹ during the past two
49 decades (Cooper et al., 2012), which could affect background surface concentrations in the West
50 (Zhang et al., 2008). There has been great interest in using satellite observations of ozone and
51 related species to monitor and attribute background surface ozone (Lin et al., 2012a; Fu et al.,
52 2013). This capability has been limited so far by the temporal sparseness of satellite data and low
53 sensitivity to the surface. All satellite measurements so far have been from low Earth orbit
54 (LEO). Here we show that multispectral measurements from the NASA Tropospheric Emissions:
55 Monitoring of Pollution (TEMPO) geostationary satellite mission over North America, scheduled
56 for launch in 2018-2019, can provide a powerful ozone monitoring resource to complement
57 surface sites, and can help to identify NAAQS exceedances caused by elevated background.

58 The North American background is defined by the EPA as the surface ozone concentration
59 that would be present over the US in the absence of North American anthropogenic emissions. It
60 includes natural sources and intercontinental pollution, and represents a floor for the achievable
61 benefits from domestic emissions control policies (including agreements with Canada and

62 Mexico). The North American background is particularly high in the Intermountain West, a
63 region extending between the Sierra Nevada/Cascades on the west and the Rocky Mountains on
64 the east, due to high elevation and arid terrain (Zhang et al., 2011). Subsidence of high-ozone air
65 from the free troposphere can cause surface ozone concentrations in that region to approach or exceed
66 the NAAQS (Reid et al., 2008). This is not an issue in the eastern US because of lower elevation,
67 forest cover, and high moisture (Fiore et al., 2002).

68 Background effects on surface ozone air quality are important to diagnose, as NAAQS
69 exceedances can be dismissed as exceptional events if shown to be not reasonably controllable
70 by local governances (EPA 2013). Monitoring of ozone in the Intermountain West is mostly
71 performed at urban stations designed to observe local pollution and not background influences.
72 There is a limited network of Clean Air Status and Trends Network (CASTNet;
73 www.epa.gov/castnet) sites located at national parks and other remote locations, and these have
74 been used extensively to estimate background ozone and evaluate models (Fiore et al., 2002;
75 Zhang et al., 2011; Lin et al., 2012b; Cooper et al., 2012). Langford et al. (2009) demonstrated
76 that transport of stratospheric air contributed to surface one-minute average ozone concentrations
77 in excess of 100 ppbv in Colorado in 1999. Analysis of ozonesonde and lidar measurements by
78 Lin et al [2012b] indicates thirteen stratospheric intrusions in spring 2010 leading to observed
79 maximum daily 8-hour average (MDA8) ozone of 70-86 ppbv at surface sites. Yates et al. (2013)
80 similarly demonstrated a stratospheric origin for a NAAQS exceedance in Wyoming in June
81 2012 by using a combination of 3-D modeling, aircraft observations, LEO satellite data, and
82 geostationary weather satellites. But the current air quality observing system is very limited in
83 its ability to (1) monitor ozone at sites prone to high background, and (2) diagnose the origin of
84 high-ozone events at these sites.

85 Several chemical transport models (CTMs) and one chemistry-climate model (CCM)
86 have been used to estimate the North American background including GEOS-Chem (Fiore et al.,
87 2003; Zhang et al., 2011), GFDL AM3 CCM (Lin et al., 2012a,b), CMAQ (Mueller and Mallard
88 2011), and CAMx (Emery et al., 2012). Values average 30-50 ppbv in spring and summer over
89 the Intermountain West with events exceeding 60 ppbv. There are large differences between
90 models reflecting variable contributions from the stratosphere (Lin et al. 2012b), lightning
91 (Kaynak et al. 2008, Zhang et al. 2011), and wildfires (Mueller and Mallard, 2011; Zhang et al.,
92 2011; Jaffe and Wigder, 2012; Singh et al., 2012).

93 Geostationary satellites are a promising tool to address the limitations of the current observing
94 system (Fishman et al., 2012; Lahoz et al., 2012). These satellites orbit the Earth with a 24-h period in
95 an equatorial plane, thus continuously staring at the same scenes. Depending on the observing strategy,
96 they may provide hourly ozone data over a continental domain, while a LEO satellite may offer at best
97 a 1-day return time. A global constellation of geostationary satellite missions targeted at air quality is
98 planned to launch in 2018-2019 including TEMPO over North America (Chance et al. 2012),
99 SENTINEL-4 over Europe (Ingmann et al., 2012), and GEMS over East Asia (Kim 2012; Bak et al.,
100 2013).

101 TEMPO will measure backscattered solar radiation in the 290-740 nm range, including
102 the ultraviolet (UV) and visible Chappuis (Vis) ozone bands (Chance et al., 1997; Liu et al.,
103 2005). Sentinel-4 and GEMS will only measure ozone in the UV. Observation in the weak
104 Chappuis band takes advantage of the relative transparency of the atmosphere in the Vis to
105 achieve sensitivity to near-surface ozone (Natraj et al., 2011; Selitto et al., 2012a). An observing

106 system simulation experiment (OSSE) by Zoogman et al. (2011) shows that a UV+Vis instrument in
107 geostationary orbit could provide useful constraints on surface ozone through data assimilation.

108 Here we conduct an OSSE to quantify the potential of geostationary ozone measurements
109 from TEMPO to improve monitoring of ozone NAAQS exceedances in the Intermountain West
110 and the role of background ozone in causing these exceedances. Our goal is to inform the TEMPO
111 observing strategy and develop methods for exploitation of TEMPO data. OSSEs have previously
112 informed mission planning for geostationary observations of atmospheric composition (Edwards et al.,
113 2009; Timmermans et al., 2009; Zoogman et al., 2011, 2014, Claeys et al., 2011, Selitto et al.,
114 2014). An important feature of our work here is the inclusion of surface network and LEO
115 satellite observations in the data assimilation system to properly quantify the added benefit of
116 TEMPO observations.

117 **2. Observing System Simulation Experiment (OSSE)**

118 OSSEs are a standard technique for assessing the information to be gained by data assimilation
119 from adding a new instrument to an existing observing system (Lord et al., 1997). The OSSE
120 framework involves the use of a model to generate synthetic time-varying 3-D fields of concentrations
121 (taken as the “true” atmosphere), and the virtual sampling of this “true” atmosphere by the different
122 instruments composing the observing system for data assimilation. This virtual sampling follows the
123 observing schedules and error characteristics of each instrument. The virtual observations are then
124 assimilated in a second, independent model, and the results of the assimilation (with and without the
125 new instrument) are compared to the “true” atmosphere to assess the value of the new instrument
126 (Edwards et al., 2009).

127 We conduct our OSSE for April-June 2010, corresponding to the seasonal maximum in
128 background ozone over the Intermountain West (Brodin et al., 2010). The observing system includes
129 the CASTNet surface network, a LEO instrument, and TEMPO. The “true” atmosphere is provided by
130 the GFDL AM3 CCM (Lin et al., 2012a,b). The model used for data assimilation (“forward model”) is
131 the GEOS-Chem CTM (Zhang et al, 2011); it generates *a priori* concentrations at successive time steps
132 to be corrected to the “true” atmosphere by the observing system through data assimilation. The
133 information provided by the observing system is quantified by the correction of the mismatch between
134 the “true” state and the *a priori*. We describe below our OSSE framework including the simulation
135 models (GFDL AM3 and GEOS-Chem), the observing system, and the data assimilation system.

136 **2.1 Simulation Models**

137 We use for our “true” atmosphere the GFDL AM3 global chemistry-climate model with
138 horizontal resolution of $1/2^\circ \times 5/8^\circ$ (latitude x longitude) nudged to reanalysis winds (Lin et al.,
139 2012a,b). This CCM was successful in reproducing background ozone variability and exceptional
140 events in the Western US during the CalNex field campaign in April-June 2010 (Lin et al., 2012b).
141 This is important because the “true” model should reproduce the characteristics of the
142 observations relevant to the OSSE. Lin et al. (2012a,b) used GFDL AM3 to investigate the effect of
143 Asian transport and stratospheric intrusions on surface ozone in the Intermountain West during April-
144 June 2010, and they quantified the ozone background through a sensitivity simulation with North
145 American anthropogenic sources shut off. Here we use 3-hourly concentrations archived from
146 their standard simulation to provide the global 3-D ozone fields of the “true” atmosphere.

147 Our forward model for data assimilation is the GEOS-Chem CTM (Bey et al., 2001;
148 <http://www.geos-chem.org>) driven by GEOS assimilated meteorological data from the NASA Global
149 Modeling and Assimilation Office (GMAO). The GEOS-Chem version used here (v8-02-03) was
150 previously described by Zhang et al. (2011) in a study of background ozone influence on the
151 Intermountain West during 2006-2008. It covers the North America domain with $1/2^\circ \times 2/3^\circ$
152 horizontal resolution ($10^\circ\text{N} - 60^\circ\text{N}$, $140^\circ\text{W} - 40^\circ\text{W}$), nested within a global domain with $2^\circ \times 2.5^\circ$
153 horizontal resolution. GEOS-Chem and GFDL AM3 have completely separate development heritages
154 and use different driving meteorological fields, chemical mechanisms, and emission inventories. This
155 independence between the two models used in the OSSE is important for a rigorous assessment
156 (Arnold and Dey 1986). The horizontal resolution of both models (~ 50 km) is adequate for
157 characterization of background ozone.

158 **Figure 1** shows the maximum daily average 8-hour (MDA8) ozone concentrations in surface
159 air for each model, averaged over April-June 2010. GFDL AM3 has higher ozone concentrations than
160 GEOS-Chem over the US as a whole and over the Intermountain West (bordered region) in particular.
161 Zhang et al. (2011) previously showed that GEOS-Chem can reproduce ozone concentrations in
162 the Intermountain West up to 70 ppbv with relatively little error, but cannot reproduce
163 exceptional events of higher concentrations. GFDL AM3 is biased high in the mean but better
164 simulates high-ozone events (Lin et al., 2012b).

165

166 2.2 Observing System and Synthetic Observations

167 Our OSSE simulates the anticipated ozone observing system over the Intermountain West
168 during operation of TEMPO. This will consist of surface measurements, LEO satellite
169 measurements, and TEMPO geostationary satellite measurements. For the LEO satellite
170 measurements we assume a future version of the Infrared Atmospheric Sounding Interferometer
171 (IASI) instrument, IASI-3, that will be launched in 2016 on the MetOp-C satellite (Clerbaux, 2009).
172 IASI retrieves ozone in the thermal infrared (TIR). We also expect to have in that time frame UV ozone
173 observations from the TROPOspheric Monitoring Instrument (TROPOMI), scheduled for LEO
174 launch in 2015 (<http://www.tropomi.eu>). TIR and UV ozone instruments have similar vertical
175 sensitivities (Zhang et al., 2010). TIR has the advantage of providing observations at night that will be
176 complementary to TEMPO.

177 CASTNet provides hourly data for 12 surface sites in the Intermountain West (Figure 1) that are
178 used for background monitoring (EPA, 2013). Although these sites are sparse, they are intended
179 to be regionally representative and exhibit significant spatial correlation (Jaffe, 2011). CASTNet
180 stations outside of the Intermountain West are not used as they do not provide useful constraints
181 for the region. CASTNet ozone measurements have 2% instrument error (EPA, 2010). There is
182 additional representation error when assimilating CASTNet data into a model due to the spatial
183 mismatch between the point where the measurement is taken and the model gridsquare mean to
184 which it is compared. We find a representation error of 5% for the $\sim 50 \times 50$ km² gridsquare size of
185 GEOS-Chem, based on the model error correlation length scale (see Section 2.4). During
186 nighttime the representation error could be much larger due to surface air stratification. Thus we
187 only assimilate CASTNet data during daytime.

188 TEMPO and IASI-3 are both nadir viewing satellite instruments, with retrieval of vertical
189 concentration profiles to be made by optimal estimation (Rodgers, 2000). If \mathbf{x}_p is the true profile,
190 i.e. the vector of true concentrations in an observation column, then the retrieved profile \mathbf{x}_p' is

191 related to \mathbf{x}_p by the instrument averaging kernel matrix \mathbf{A} which defines the sensitivity of \mathbf{x}_p' to
192 \mathbf{x}_p ($\mathbf{A} = \partial\mathbf{x}_p'/\partial\mathbf{x}_p$):

$$193 \quad \mathbf{x}_p' = \mathbf{x}_s + \mathbf{A}(\mathbf{x}_p - \mathbf{x}_s) + \boldsymbol{\varepsilon} \quad (1)$$

194 where $\boldsymbol{\varepsilon}$ is the instrument noise vector and \mathbf{x}_s is an independent *a priori* ozone profile used to
195 regularize the retrieval.

196 **Figure 2** shows typical clear-sky averaging kernel matrices for UV+Vis and TIR retrievals of
197 tropospheric ozone taken from the Natraj et al. (2011) theoretical study. Also shown are the degrees
198 of freedom for signal (DOFS) below given pressure levels. The DOFS are the number of independent
199 pieces of information in the vertical provided by the retrieval, as determined from the corresponding
200 trace of the averaging kernel matrix. The UV+Vis spectral ranges (290-340 nm, 560-620 nm) and
201 spectral resolution (0.4 nm) assumed by Natraj et al. (2011) are comparable to the spectral ranges
202 (290-490 nm, 540-740 nm) and spectral resolution (0.6 nm) planned for TEMPO. The additional
203 near-surface information provided by the UV+Vis combination is consistent with previous work
204 using SCIAMACHY data (Selitto et al., 2012b).

205 We generate synthetic TEMPO geostationary observations from the GFDL AM3 “true”
206 atmosphere by sampling daytime vertical profiles over land in the North American domain with the
207 averaging kernel matrix given in **Figure 2**. TEMPO observations over the ocean are not included as the
208 planned field of regard for the mission includes very little ocean and because the clear ocean surface is
209 too dark for Vis retrievals. We similarly generate synthetic LEO IASI-3 (henceforth LEO) observations
210 over the North American domain twice a day (local noon and midnight) with the averaging kernel
211 matrix given in **Figure 2**. We omit scenes with cloud fraction > 0.3 (as given by the GEOS
212 meteorological data). We assume fixed averaging kernel matrices, acknowledging that in practice
213 there is significant variability (Worden et al., 2013). Gaussian noise is added to the synthetic
214 observations following Natraj et al. (2011) to simulate the random error associated with the spectral
215 measurement. The noise from the TEMPO instrument (footprint of $4 \times 8 \text{ km}^2$) is reduced by the square
216 root of the number of observations averaged over each GEOS-Chem grid square ($\sim 50 \times 50 \text{ km}^2$) in the
217 data assimilation process. Since the TEMPO measurements are spatially dense we assume zero
218 representation error during assimilation. Current IASI measurements have footprint diameters of 12-40
219 km with centers spaced 25-80 km apart (August et al., 2012); no reduction of the random error is
220 applied to the LEO observations.

221 **2.3 Assimilation of surface and satellite measurements**

222 The goal of our data assimilation system is to optimize an n -element state vector (\mathbf{x}) of 3-
223 D tropospheric ozone concentrations over the North American domain of GEOS-Chem, using
224 surface and satellite observations to correct the GEOS-Chem simulation at successive time steps.
225 CASTNet and TEMPO data are assimilated at discrete 3-h time steps, and LEO data are
226 assimilated at 12-h time steps. We use a Kalman filter, as previously applied to ozone data
227 assimilation by Khattatov et al (2000), Parrington et al. (2008), and Zoogman et al. (2011). At
228 each time step, we calculate an optimal estimate $\hat{\mathbf{x}}$ of the true ozone concentrations \mathbf{x} as a weighted
229 average of the model forecast \mathbf{x}_a (with corresponding error vector $\boldsymbol{\varepsilon}_a$ relative to the true concentrations)
230 and the observations \mathbf{x}' (with observational error $\boldsymbol{\varepsilon}'$ and with \mathbf{x}' set to \mathbf{x}_a where there are no
231 observations). The observational error includes both the instrument noise $\boldsymbol{\varepsilon}$ and (for surface sites) the

232 previously defined representation error. The errors are characterized by error covariance matrices $\mathbf{S}_a =$
 233 $E[\boldsymbol{\varepsilon}_a \boldsymbol{\varepsilon}_a^T]$ and $\mathbf{S}_\varepsilon = E[\boldsymbol{\varepsilon}' \boldsymbol{\varepsilon}'^T]$, where $E[]$ is the expected-value operator. Assuming Gaussian error
 234 distributions for $\boldsymbol{\varepsilon}_a$ and $\boldsymbol{\varepsilon}$ we obtain (Rodgers, 2000):

$$235 \quad \hat{\mathbf{x}} = \mathbf{x}_a + \mathbf{G}(\mathbf{x}' - \mathbf{K}\mathbf{x}_a) \quad (2)$$

236 where \mathbf{K} is the observation operator that maps the model forecast to the observations. For satellite
 237 measurements $\mathbf{K}\mathbf{x}_a = \mathbf{x}_s + \mathbf{A}(\mathbf{x}_a - \mathbf{x}_s)$ (equation (1) with no noise term), while for surface measurements
 238 $\mathbf{K}\mathbf{x}_a = \mathbf{x}_a$. The gain matrix \mathbf{G} is given by

$$239 \quad \mathbf{G} = \mathbf{S}_a \mathbf{K}^T (\mathbf{K} \mathbf{S}_a \mathbf{K}^T + \mathbf{S}_\varepsilon)^{-1} \quad (3)$$

240 and determines the relative weight given to the observations and the model. The instrument error
 241 covariance matrix \mathbf{S}_ε is assumed diagonal and set to an arbitrarily large number in locations
 242 where there are no observations. For surface measurements we include the 5% representation
 243 error in quadrature with the 2% instrument error so that the corresponding error variances are
 244 additive. The optimal estimate $\hat{\mathbf{x}}$ has error $\hat{\boldsymbol{\varepsilon}}$ with error covariance $\hat{\mathbf{S}} = E[\hat{\boldsymbol{\varepsilon}} \hat{\boldsymbol{\varepsilon}}^T]$:

$$245 \quad \hat{\mathbf{S}} = (\mathbf{I}_n - \mathbf{G}\mathbf{K})\mathbf{S}_a \quad (4)$$

246 Where \mathbf{I}_n is the identity matrix of dimension n .

247 The model error covariance matrix \mathbf{S}_a expresses the error in the forward model at each
 248 assimilation time step and is given by:

$$249 \quad \mathbf{S}_a = \begin{pmatrix} \text{var}(\boldsymbol{\varepsilon}_{a,1}) & \cdots & \text{cov}(\boldsymbol{\varepsilon}_{a,1}, \boldsymbol{\varepsilon}_{a,n}) \\ \vdots & \ddots & \vdots \\ \text{cov}(\boldsymbol{\varepsilon}_{a,n}, \boldsymbol{\varepsilon}_{a,1}) & \cdots & \text{var}(\boldsymbol{\varepsilon}_{a,n}) \end{pmatrix} \quad (5)$$

250 where $\boldsymbol{\varepsilon}_a = (\boldsymbol{\varepsilon}_{a,1}, \dots, \boldsymbol{\varepsilon}_{a,n})^T$, with $\boldsymbol{\varepsilon}_{a,i}$ representing the error for GEOS-Chem gridbox i . Following
 251 Zoogman et al. (2011), we initialize \mathbf{S}_a at the beginning of the simulation as a diagonal matrix
 252 with *a priori* errors of 29%, and update it at each assimilation time step on the basis of the
 253 computed *a posteriori* error covariance matrix $\hat{\mathbf{S}}$ (equation (4)). The diagonal terms of $\hat{\mathbf{S}}$ are
 254 transported as tracers in GEOS-Chem to the next assimilation time step and are augmented by a model
 255 error variance reflecting the time-dependent divergence of the model from the true state (Zoogman et
 256 al., 2011). This yields the diagonal terms $\text{var}(\boldsymbol{\varepsilon}_{a,i})$ of \mathbf{S}_a for the next assimilation time step. The
 257 off-diagonal terms (error covariances) describe the propagation of information from each
 258 observation over a spatial domain of influence. We compute $\text{cov}(\boldsymbol{\varepsilon}_{a,i}, \boldsymbol{\varepsilon}_{a,j})$ for each pair of
 259 gridboxes (i,j) as a function of the horizontal and vertical distance between the two gridboxes
 260 using the error correlation length scales from section 2.4.

261 In practice the dimension of the matrices used in the assimilation must be limited to make
 262 the computation tractable. This is done by solving (2) column by column and including only
 263 measurements at a horizontal distance less than 510 km (the horizontal error correlation length
 264 scale, see below) in the model error covariance matrix.

265

266 2.4 Error Correlation Length Scales

267 The spatial extent of information provided by an observation to correct the GEOS-Chem
268 model simulation through data assimilation can be quantified by correlating the GEOS-Chem
269 errors relative to *in situ* observations at different sites in the Intermountain West (for the
270 horizontal scale) and ozonesonde profiles (for the vertical scale). To define a horizontal error
271 correlation length scale we used actual CASTNet surface measurements from our period of study
272 (April-June 2010), downloaded from <http://epa.gov/castnet/>. We compute the time series of
273 model error during daytime (0900 – 1700 LT) at each surface site, and from there derive the
274 model error correlation between each pair of surface sites. **Figure 3 (left)** shows the correlation
275 coefficients plotted against the distance d between sites (binned every 100km). We find $R=\exp(-$
276 $d/510$ km). We also show the error correlation length scale calculated when comparing GEOS-
277 Chem and GFDL AM3 (in red) sampled over the Intermountain West region. The model-model
278 error correlation length scale is similar to the model-observation length scale, providing support
279 for the realism of error patterns in our OSSE. We assume that the horizontal error correlation
280 length scale is invariant with altitude.

281 To estimate the vertical correlation length scale we compare GEOS-Chem ozone
282 concentrations to *in situ* vertical profiles from May-June 2010 ozonesondes at six locations in
283 California (Cooper et al. 2011). **Figure 3 (right)** shows the correlation coefficients plotted
284 against the vertical distance z (binned every 500 m) for the time series of model errors at each
285 ozonesonde station from the surface to 8 km altitude. We find $R=\exp(-z/1.7$ km). Again, the
286 model-model length scale (red) is not significantly different from the model-observation length
287 scale.

288

289 3. TEMPO observation of high-ozone events in the Intermountain West

290 We now apply our OSSE system to evaluate the benefit of TEMPO observations to
291 monitor and attribute ozone exceedances in the Intermountain West. We compare the “true”
292 concentrations in surface air over the Intermountain West to GEOS-Chem CTM ozone
293 concentrations without data assimilation (*a priori*) and with assimilation of synthetic CASTNet,
294 TEMPO, and IASI-3 LEO observations. We also performed an assimilation of CASTNet and
295 TEMPO observations without a LEO instrument and found no significant difference in results.
296 Thus the LEO instrument does not add significant information beyond TEMPO for constraining
297 surface ozone concentrations in the Intermountain West. Its value for tracking exceptional events
298 will be discussed in section 4.

299 **Figure 4** examines the ability of the data assimilation system to monitor daily MDA8
300 ozone over the Intermountain West at the $1/2^\circ \times 2/3^\circ$ ($\sim 50 \times 50$ km²) GEOS-Chem grid resolution.
301 The top panel shows a scatterplot of *a priori* GEOS-Chem MDA8 ozone concentrations in April-
302 June 2010, for individual grid squares over the Intermountain West domain of Figure 1 and
303 individual days, vs. the “true” concentrations from the GFDL AM3 model. The GEOS-Chem *a*
304 *priori* is biased low and performs poorly in reproducing the “true” variability ($R^2=0.12$, bias = -
305 9.0 ppbv). Assimilation of synthetic CASTNet surface measurements reduces the low bias from
306 9.0 to 2.8 ppbv, but still does not capture much of the variability ($R^2=0.34$). Adding the synthetic
307 TEMPO geostationary observations eliminates the low bias and captures over half of the
308 variability ($R^2=0.58$).

309 The ability of TEMPO observations to capture high-ozone events is of particular interest.
310 **Figure 5** shows a map of the number of days in April-June 2010 with MDA8 ozone in excess of
311 70 ppbv for individual GEOS-Chem gridsquares in the Intermountain West. Values are shown
312 for the “true” atmosphere, the GEOS-Chem *a priori* without data assimilation, and the data
313 assimilation results including only the CASTNet observations and with the addition of TEMPO
314 observations. The “truth” shows an average of 5.7 high-ozone events per gridsquare in the
315 Intermountain West over the April-June 2010 period. The *a priori* model has only 0.8 event-days
316 per gridsquare and the spatial pattern is very different (spatial correlation $R^2=0.09$ for the
317 ensemble of Intermountain West gridsquares). Assimilation of surface measurements improves
318 both the average number of high-ozone events (3.6 event-days) and the spatial pattern ($R^2=0.62$).
319 The inability to fully correct the bias is due in part to the large impact of free tropospheric air in
320 driving high-ozone events, and in part to the limited coverage from the sparse surface network.
321 Adding TEMPO satellite observations almost fully corrects the bias (mean of 5.4 event-days)
322 and captures most of the spatial distribution of high-ozone events ($R^2=0.82$).
323

324 **4. Attribution of exceptional events using TEMPO observations**

325 TEMPO will provide continuous daytime observation in the free troposphere as well as in
326 the boundary layer, with separation between the two (Figure 2). Thus it could be particularly
327 powerful in quantifying free tropospheric background contributions to NAAQS exceedances.
328 This would assist in the designation of exceptional events where an exceedance of the NAAQS is
329 considered to be outside local control.

330 We examine a case study of a stratospheric intrusion on June 13 in the GFDL AM3
331 model taken as the “truth”. **Figure 6** shows a time series for June 2010 of MDA8 ozone
332 concentrations at a location in northern New Mexico (107°W, 36°N). We choose this event as it
333 was diagnosed by ozonesonde observations and meteorological tracers as a deep stratospheric
334 intrusion event (Lin et al., 2012a). Actual observations at nearby CASTNet locations indicate
335 ozone in excess of 75 ppbv during this modeled intrusion.

336 Evidence of free tropospheric origin for the June 13 event is critical to achieving an
337 “exceptional event” designation. **Figure 7** (top left) shows a longitude-altitude cross section of
338 ozone concentrations in the GFDL AM3 model taken as the “truth”. The stratospheric intrusion
339 is manifest at 103-109°W. The *a priori* GEOS-Chem model (top right) also shows a stratospheric
340 ozone enhancement extending to the surface but of much smaller magnitude. Assimilation of
341 surface measurements (not shown) makes little correction in the free troposphere. Synthetic
342 satellite measurement imagery from TEMPO without assimilation (bottom left) shows elevated
343 values in the free troposphere but does not properly represent surface gradients due to instrument
344 smoothing. Assimilating TEMPO observations into the GEOS-Chem CTM together with LEO
345 measurements (bottom right) captures the magnitude and spatial structure of the stratospheric
346 intrusion, and this would make a strong case for diagnosis of an exceptional event. We see here
347 that the use of data assimilation efficiently enhances the information from TEMPO to constrain
348 surface air concentrations. Information from the LEO instrument does not add significantly in
349 this case to observations from TEMPO, although it does correct ozone fields over the ocean
350 where TEMPO does not observe in this OSSE. The LEO instrument will thus be valuable for
351 tracking transpacific transport of ozone plumes even when TEMPO is operational.
352

353 **5. Summary**

354 We demonstrated the potential of future TEMPO UV+Vis geostationary observations to
355 monitor ozone exceedances in the Intermountain West and identify those exceedances caused by
356 the North American background. Our goal was to inform the TEMPO observing strategy and
357 develop methods for exploitation of its data. To accomplish this we performed an observation system
358 simulation experiment (OSSE) for assimilation of the TEMPO data using two global 3-D ozone
359 models with ~50 km horizontal resolution, one as the “true” atmosphere and one as the forward model
360 for data assimilation. We also included in our OSSE surface measurements from the current CASTNet
361 monitoring network sites in the Intermountain West (12 sites) and satellite measurements from a
362 thermal infrared (TIR) low Earth orbit (LEO) instrument projected to be in orbit concurrently with
363 TEMPO.

364 An important factor in data assimilation is the scales over which observed information
365 can be propagated with the forward model. We quantified this using model error correlation
366 length scales for the Intermountain West based on actual CASTNet and ozonesonde data. We
367 find length scales of 500 km (horizontal) and 1.7 km (vertical). These are in close agreement
368 with error correlation length scales between the two models used in our OSSE.

369 We find that the CASTNet surface observations are too sparse to adequately monitor
370 high-ozone events in the Intermountain West even after data assimilation. We show that the
371 TEMPO geostationary observations will provide a greatly improved observing system for
372 monitoring such events. In addition, because of the information they provide on the vertical
373 distribution of ozone, they can effectively diagnose NAAQS exceedances caused by background
374 ozone. A LEO satellite instrument flying concurrently with TEMPO provide no significant added
375 value for monitoring the ozone background over the US but could be useful for tracking
376 transpacific plumes.

377 The use of invariant averaging kernel matrices is a limitation of this study. Preparation
378 for TEMPO must include improved constraints on physical parameters, such as surface albedo,
379 that can vary greatly over the North American domain and that affect the sensitivity of UV+Vis
380 retrievals of near-surface ozone. Also, if the differences between the two models used in our
381 OSSE are larger than future errors in modeled ozone, this study may overestimate the
382 information TEMPO will provide.

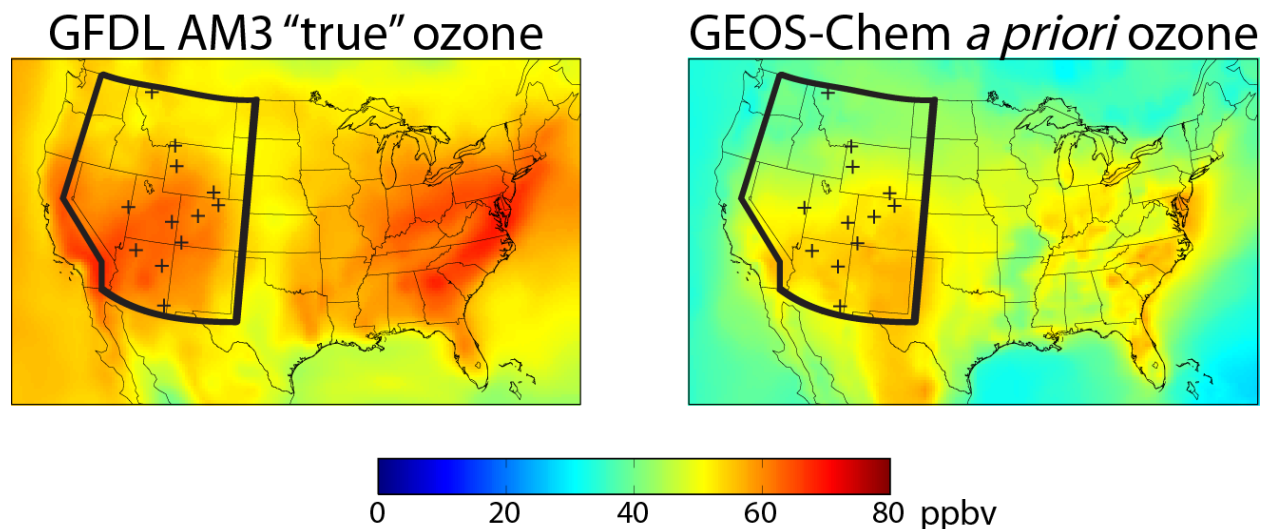
383 Use of the complete observing system described here (surface, geostationary, and LEO)
384 will provide a powerful tool for future air quality policy. Planning is underway to combine this
385 system with regional air quality models to supply the public with near real time pollution reports
386 and forecasts. These reports and forecasts would be much the same as currently available
387 weather information, also provided in large part from geostationary satellite observations.

388

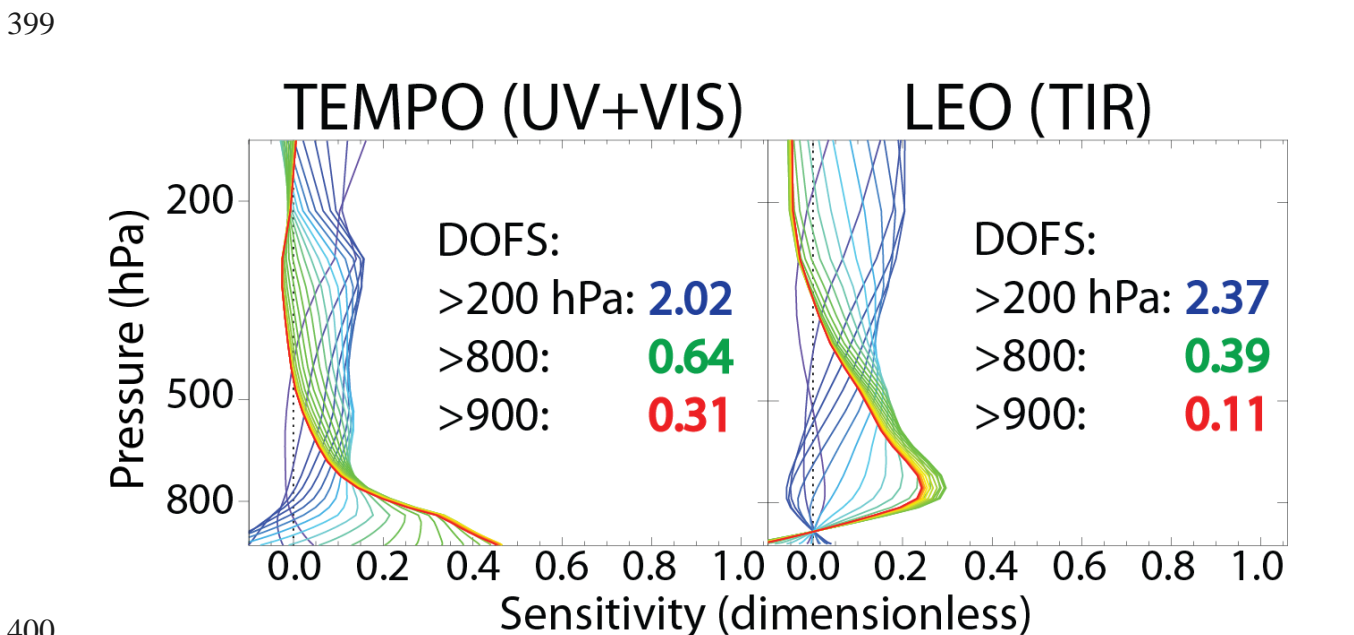
389 **Acknowledgements:** This work was supported by the NASA Earth Science Division and by a NASA
390 Earth and Space Science Fellowship to Peter Zoogman.

391

392 **Figures:**



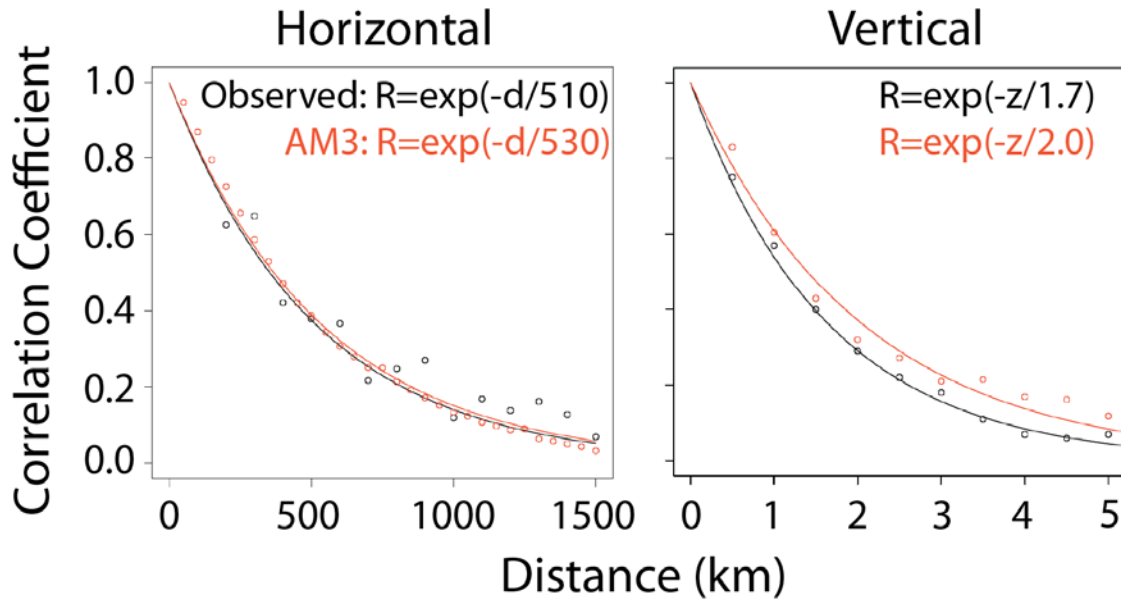
393
 394 **Figure 1:** Mean values of the daily maximum 8-hour average (MDA8) ozone concentrations for
 395 April-June 2010 in surface air. Left panel shows values from the GFDL AM3 CCM used as the
 396 “true” atmosphere in our OSSE. Right panel shows the *a priori* values from the GEOS-Chem
 397 CTM used for data assimilation. The black lines delineate the Intermountain West and black
 398 crosses show CASTNet surface measurement sites in the region.



400
 401 **Figure 2:** Averaging kernel matrices assumed in this study (from Natraj et al. [2011]) for clear-
 402 sky retrievals of tropospheric ozone from space in the UV+Vis (left) and the TIR (right).
 403 UV+Vis in our study corresponds to TEMPO, while TIR corresponds to a future LEO instrument
 404 flying concurrently with TEMPO. Lines are matrix rows for individual vertical levels, with the color
 405 gradient from red to blue corresponding to vertical levels ranging from surface air (red) to 200 hPa

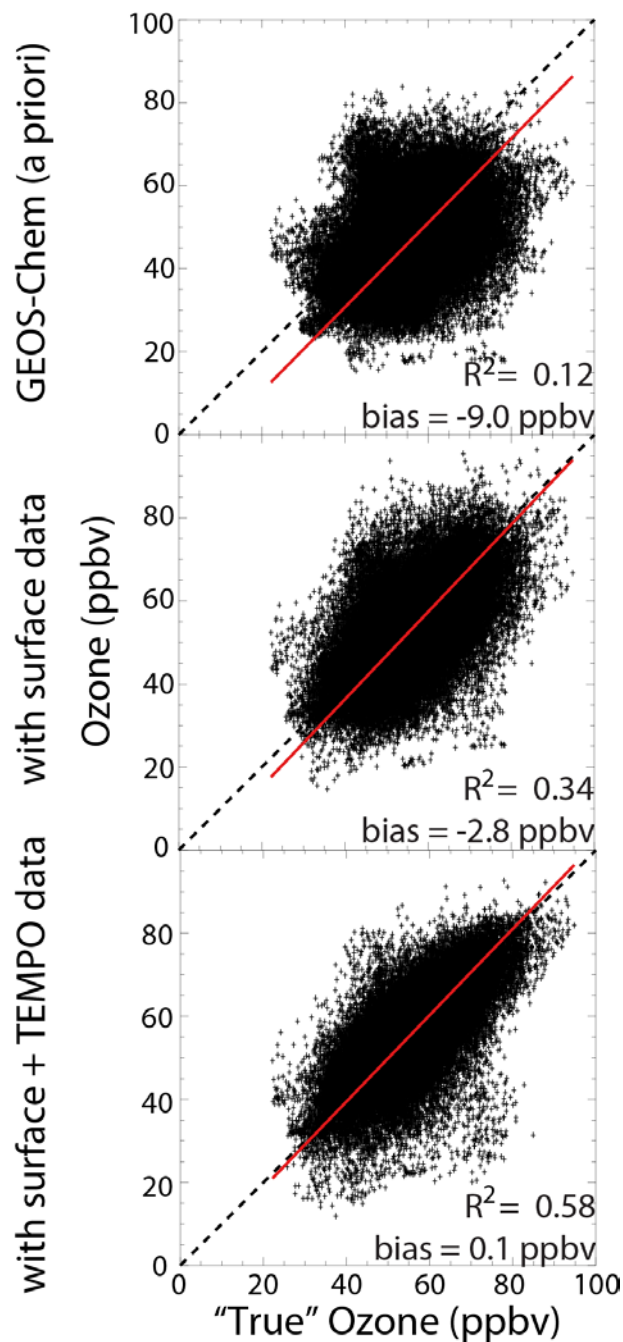
406 (blue). Inset are the degrees of freedom for signal (DOFS) for the atmospheric columns below 200,
407 800, and 900 hPa.

408



409

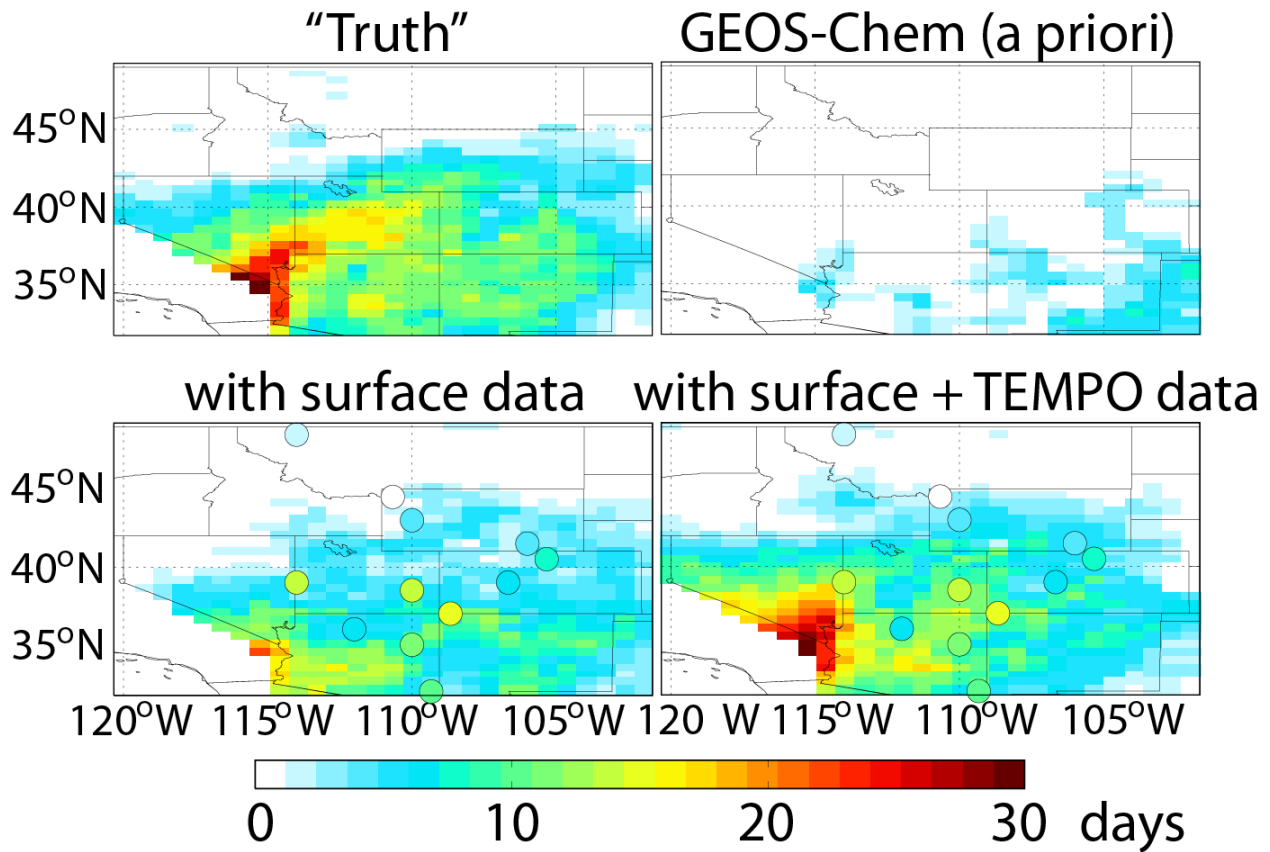
410 **Figure 3:** Error correlation length scales for the GEOS-Chem model simulation of tropospheric
411 ozone in the US Intermountain West. The error correlations are relative to actual CASTNet and
412 ozonesonde observations (in black) and relative to the GFDL AM3 model sampled in the
413 Intermountain West region (in red). Statistics are computed for April-June 2010. The left panel
414 shows the correlation coefficient (R) of the model error between pairs of CASTNet sites, plotted
415 against the distance between sites. Values are for the 12 CASTNet sites in the Intermountain
416 West (Figure 1). The right panel shows the correlation coefficient of the model error between
417 pairs of vertical levels (up to 8 km altitude) for ozonesonde measurements from the IONS-2010
418 campaign in California [Cooper et al. 2011], plotted against distance between levels.
419 Exponential fits to the data are shown inset, where d and z are horizontal and vertical distances in
420 km.



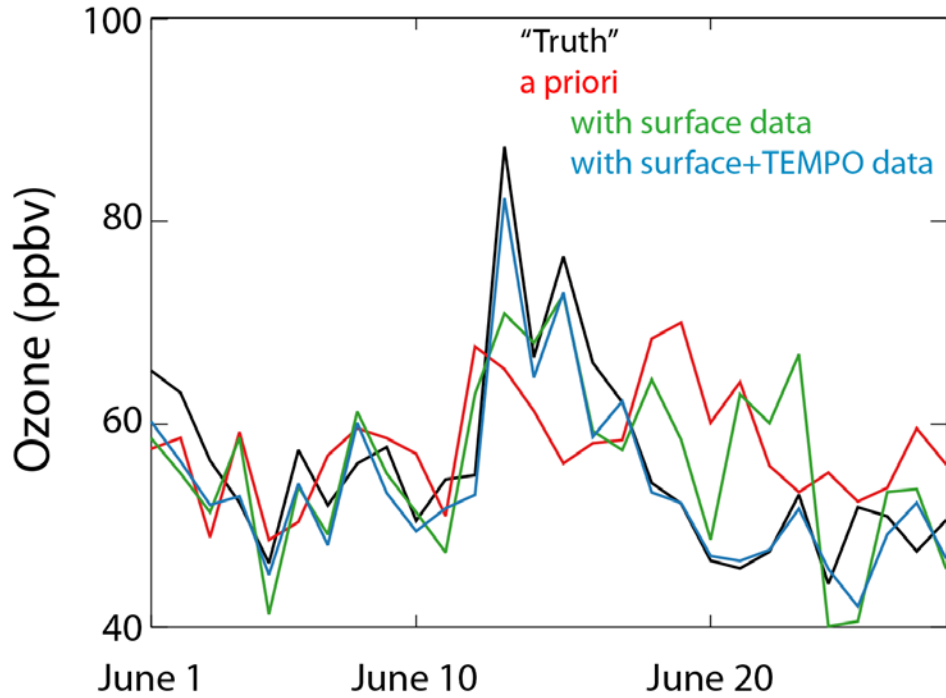
421

422 **Figure 4:** Improved monitoring of surface ozone across the Intermountain West from
 423 assimilation of synthetic CASTNet (surface) and TEMPO (geostationary satellite) observations.
 424 The figure shows scatterplots of simulated (GEOS-Chem) vs. "truth" (GFDL AM3) daily
 425 maximum 8-h (MDA8) surface ozone for April-June 2010 for all $1/2^\circ \times 2/3^\circ$ grid squares in the
 426 region (Figure 1) and for individual days. Results are for GEOS-Chem without data assimilation
 427 (top), with assimilation of CASTnet synthetic surface data (middle), and with additional
 428 assimilation of TEMPO and LEO synthetic satellite data (bottom). Comparison statistics are
 429 inset. Also shown are the reduced-major-axis (RMA) regression line and the 1:1 line.

Number of days with MDA8 ozone > 70 ppbv

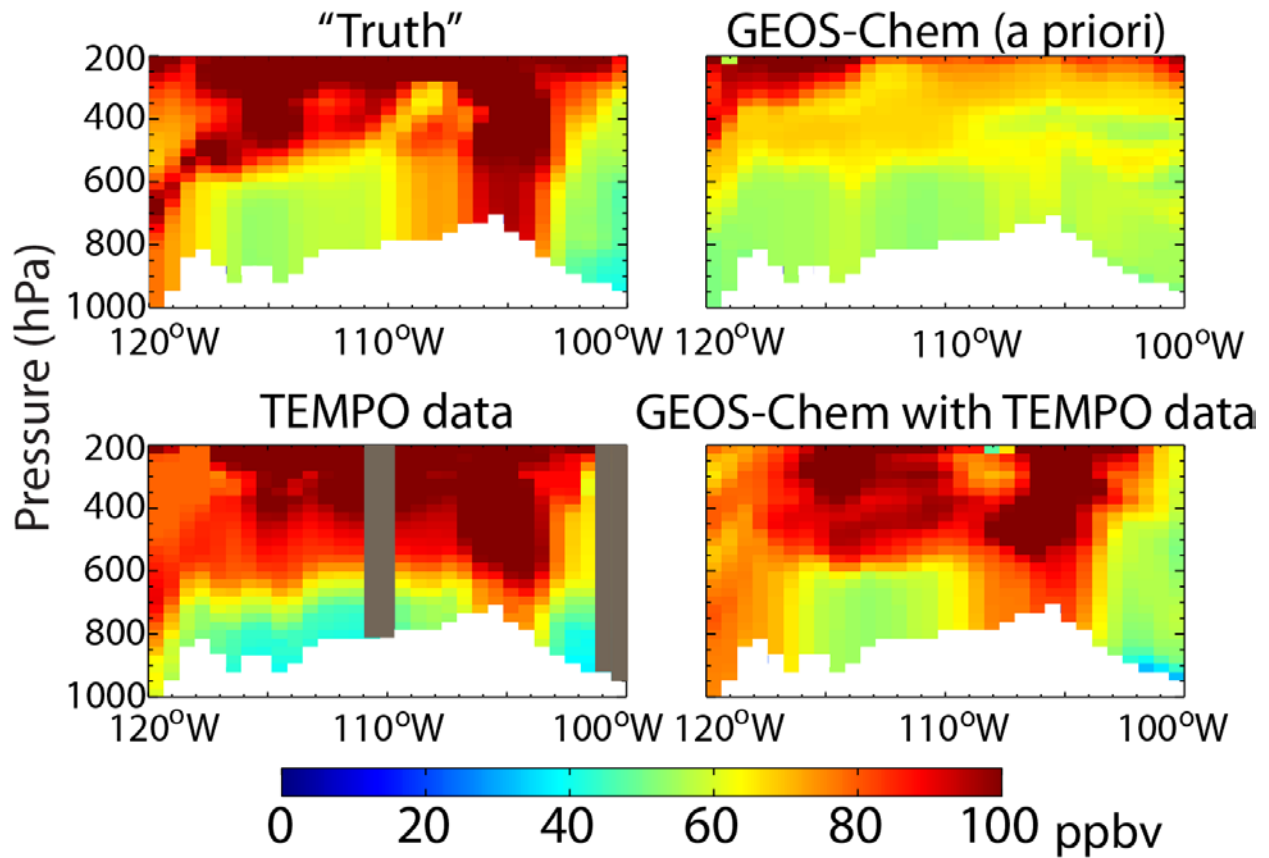


431 **Figure 5:** Improved detection of high-ozone events in the Intermountain West by data
432 assimilation. The figure shows the number of events (daily maximum 8-h ozone > 70 ppbv) in
433 April-June 2010 on the GEOS-Chem grid. The “truth” defined by the GFDL AM3 model (top
434 left panel) is compared to GEOS-Chem simulations without data assimilation (top right), with
435 assimilation of synthetic CASTNet surface data (bottom left), and with additional assimilation of
436 synthetic TEMPO and LEO satellite data (bottom right). Locations of CASTNet surface sites
437 used for assimilation with their “true” values are overlain in the bottom panels.
438



439
 440
 441
 442
 443
 444
 445
 446

Figure 6: Detection of an exceptional ozone event by TEMPO. The Figure shows the June 2010 time series of daily maximum 8-h (MDA8) ozone concentrations at a location in northern New Mexico (107°W, 36°N) featuring a major stratospheric intrusion on June 13 in the GFDL AM3 model taken as the “truth” (black line). The ability to capture this event is examined for the GEOS-Chem model without data assimilation (a priori, red line) and with assimilation of surface measurements only (green line) and satellite measurements added (blue line).



447
 448 **Figure 7:** Longitude-altitude cross-section of ozone concentrations (36°N, 2100 MT on June 13,
 449 2010) associated with the stratospheric intrusion of Figure 6. The “true” state from the GFDL
 450 AM3 model (top left) is compared to the GEOS-Chem model without data assimilation (top
 451 right) and with assimilation of surface and satellite data (bottom right). The bottom left panel
 452 shows synthetic TEMPO observations of the “true” state (gray regions indicate cloudy scenes)
 453 without data assimilation. Local topography is shown in white.

454 **References:**

- 455 Arnold, C. and Dey, C., 1986. Observing-systems simulation experiments - past, present, and
456 future. *Bulletin of the American Meteorological Society* 67, 687-695.
- 457 August, T., Klaes, D., Schluessel, P., Hultberg, T., Crapeau, M., Arriaga, A., O'Carroll, A.,
458 Coppens, D., Munro, R., Calbet, X., 2012. IASI on metop-A: Operational level 2
459 retrievals after five years in orbit. *Journal of Quantitative Spectroscopy & Radiative*
460 *Transfer* 113, 1340-1371.
- 461 Bak, J., Kim, J.H., Liu, X., Chance, K., Kim, J., 2013. Evaluation of ozone profile and
462 tropospheric ozone retrievals from GEMS and OMI spectra. *Atmospheric Measurement*
463 *Techniques* 6, 239-249.
- 464 Bey, I., Jacob, D., Yantosca, R., Logan, J., Field, B., Fiore, A., Li, Q., Liu, H., Mickley, L.,
465 Schultz, M., 2001. Global modeling of tropospheric chemistry with assimilated
466 meteorology: Model description and evaluation. *Journal of Geophysical Research-*
467 *Atmospheres* 106, 23073-23095.
- 468 Brodin, M., Helmig, D., Oltmans, S., 2010. Seasonal ozone behavior along an elevation gradient
469 in the colorado front range mountains. *Atmospheric Environment* 44, 5305-5315.
- 470 Chance, K., Lui, X., Suleiman, R.M., Flittner, D.E., Janz, S.J., 2012. Tropospheric Emissions:
471 Monitoring of Pollution (TEMPO). Abstract A31B-0020 presented at the 2012 AGU Fall
472 Meeting.
- 473 Chance, K., Burrows, J., Perner, D., Schneider, W., 1997. Satellite measurements of atmospheric
474 ozone profiles, including tropospheric ozone, from ultraviolet/visible measurements in
475 the nadir geometry: A potential method to retrieve tropospheric ozone. *Journal of*
476 *Quantitative Spectroscopy & Radiative Transfer* 57, 467-476.
- 477 Claeysman, M., Attie, J-L., Peuch, V-H., El Amraoui, L., Lahoz, W.A., Josse, B., Joly, M., Barre,
478 J., Ricaud, P., Massart, S., Piacentini, A., von Clarmann, T., Hopfner, M., Orphal, J.,
479 Flaud, J.M., Edwards, D.P., 2011. A thermal infrared instrument onboard a geostationary
480 platform for CO and O-3 measurements in the lowermost troposphere: Observing System
481 Simulation Experiments (OSSE). *Atm. Meas. Tech.*, 4, 1637-1661.
- 482 Clerbaux, C., Boynard, A., Clarisse, L., George, M., Hadji-Lazaro, J., Herbin, H., Hurtmans, D.,
483 Pommier, M., Razavi, A., Turquety, S., Wespes, C., Coheur, P.-., 2009. Monitoring of
484 atmospheric composition using the thermal infrared IASI/MetOp sounder. *Atmospheric*
485 *Chemistry and Physics* 9, 6041-6054.
- 486 Cooper, O.R., Oltmans, S.J., Johnson, B.J., Brioude, J., Angevine, W., Trainer, M., Parrish,
487 D.D., Ryerson, T.R., Pollack, I., Cullis, P.D., Ives, M.A., Tarasick, D.W., Al-Saadi, J.,
488 Stajner, I., 2011. Measurement of western US baseline ozone from the surface to the

- 489 tropopause and assessment of downwind impact regions. *Journal of Geophysical*
490 *Research-Atmospheres* 116, D00V03.
- 491 Cooper, O.R., Gao, R., Tarasick, D., Leblanc, T., Sweeney, C., 2012. Long-term ozone trends at
492 rural ozone monitoring sites across the United States, 1990-2010. *Journal of Geophysical*
493 *Research-Atmospheres* 117, D22307.
- 494 Edwards, D.P., Arellano, A.F., Jr., Deeter, M.N., 2009. A satellite observation system simulation
495 experiment for carbon monoxide in the lowermost troposphere. *Journal of Geophysical*
496 *Research-Atmospheres* 114, D14304.
- 497 Emery, C., Jung, J., Downey, N., Johnson, J., Jimenez, M., Yarvwood, G., Morris, R., 2012.
498 Regional and global modeling estimates of policy relevant background ozone over the
499 United States. *Atmospheric Environment* 47, 206-217.
- 500 Fiore, A., Jacob, D., Liu, H., Yantosca, R., Fairlie, T., Li, Q., 2003. Variability in surface ozone
501 background over the United States: Implications for air quality policy. *Journal of*
502 *Geophysical Research-Atmospheres* 108, 4787.
- 503 Fiore, A., Jacob, D., Bey, I., Yantosca, R., Field, B., Fusco, A., Wilkinson, J., 2002. Background
504 ozone over the United States in summer: Origin, trend, and contribution to pollution
505 episodes. *Journal of Geophysical Research-Atmospheres* 107, 4275.
- 506 Fishman, J., Iraci, L.T., Al-Saadi, J., Chance, K., Chavez, F., Chin, M., Coble, P., Davis, C.,
507 DiGiacomo, P.M., Edwards, D., Eldering, A., Goes, J., Herman, J., Hu, C., Jacob, D.J.,
508 Jordan, C., Kawa, S.R., Key, R., Liu, X., Lohrenz, S., Mannino, A., Natraj, V., Neil, D.,
509 Neu, J., Newchurch, M., Pickering, K., Salisbury, J., Sosik, H., Subramaniam, A.,
510 Tzortziou, M., Wang, J., Wang, M., 2012. The united states' next generation of
511 atmospheric composition and coastal ecosystem measurements NASA's geostationary
512 coastal and air pollution events (GEO-CAPE) mission. *Bulletin of the American*
513 *Meteorological Society* 93, 1547-+.
- 514 Fu, D., Worden, J.R., Liu, X., Kulawik, S.S., Bowman, K.W., Natraj, V., 2013. Characterization
515 of ozone profiles derived from aura TES and OMI radiances. *Atmospheric Chemistry and*
516 *Physics* 13, 3445-3462.
- 517 Ingmann, P., Veihelmann, B., Langen, J., Lamarre, D., Stark, H., Courreges-Lacoste, G.B., 2012.
518 Requirements for the GMES atmosphere service and ESA's implementation concept:
519 Sentinels-4/-5 and-5p. *Remote Sensing of Environment* 120, 58-69.
- 520 Jaffe, D., 2011. Relationship between surface and free tropospheric ozone in the western U.S.
521 *Environmental science & technology* 45, 432-438.
- 522 Jaffe, D.A. and Wigder, N.L., 2012. Ozone production from wildfires: A critical review.
523 *Atmospheric Environment* 51, 1-10.

- 524 Kaynak, B., Hu, Y., Martin, R.V., Russell, A.G., Choi, Y., Wang, Y., 2008. The effect of
525 lightning NO_x production on surface ozone in the continental united states. *Atmospheric*
526 *Chemistry and Physics* 8, 5151-5159.
- 527 Khattatov, B., Lamarque, J., Lyjak, L., Menard, R., Levelt, P., Tie, X., Brasseur, G., Gille, J.,
528 2000. Assimilation of satellite observations of long-lived chemical species in global
529 chemistry transport models. *Journal of Geophysical Research-Atmospheres* 105, 29135-
530 29144.
- 531 Kim, J., 2012. GEMS (Geostationary Enviroment Monitoring Spectrometer) onboard the
532 GeoKOMPSAT to monitor air quality in high temporal and spatial resolution over Asia-
533 Pacific region. Abstract EGU2012-4051 presented at the 2012 EGU General Assembly.
- 534 Lahoz, W.A., Peuch, V.-H., Orphal, J., Attie, J.-L., Chance, K., Liu, X., Edwards, D., Elbern, H.,
535 Flaud, J.-M., Claeysman, M., El Amraoui, L., 2012. Monitoring air quality from space: the
536 case for the geostationary platform. *Bulletin of the American Meteorological Society* 11,
537 221-233.
- 538 Langford, A.O., Aikin, K.C., Eubank, C.S., Williams, E.J., 2009. Stratospheric contribution to
539 high surface ozone in Colorado during springtime. *Geophysical Research Letters* 36,
540 L12801.
- 541 Lefohn, A., Oltmans, S., Dann, T., Singh, H., 2001. Present-day variability of background ozone
542 in the lower troposphere. *Journal of Geophysical Research-Atmospheres* 106, 9945-9958.
- 543 Lin, M., Fiore, A.M., Cooper, O.R., Horowitz, L.W., Langford, A.O., Levy, Hiram, II, Johnson,
544 B.J., Naik, V., Oltmans, S.J., Senff, C.J., 2012. Springtime high surface ozone events
545 over the western United States: Quantifying the role of stratospheric intrusions. *Journal*
546 *of Geophysical Research-Atmospheres* 117, D00V22.
- 547 Lin, M., Fiore, A.M., Horowitz, L.W., Cooper, O.R., Naik, V., Holloway, J., Johnson, B.J.,
548 Middlebrook, A.M., Oltmans, S.J., Pollack, I.B., Ryerson, T.B., Warner, J.X.,
549 Wiedinmyer, C., Wilson, J., Wyman, B., 2012. Transport of asian ozone pollution into
550 surface air over the western United States in spring. *Journal of Geophysical Research-*
551 *Atmospheres* 117, D00V07.
- 552 Liu, X., Sioris, C., Chance, K., Kurosu, T., Newchurch, M., Martin, R., Palmer, P., 2005.
553 Mapping tropospheric ozone profiles from an airborne ultraviolet-visible spectrometer.
554 *Applied Optics* 44, 3312-3319.
- 555 Lord, S.J., Kalnay E., Daley R., Emmitt G.D., Atlas R., 1997. Using OSSEs in the design of future g
556 eneration integrated observing systems. Preprints, 1st Symposium on Integrated Observing
557 Systems, Long Beach, CA, AMS, 45-47.

558 Mueller, S.F. and Mallard, J.W., 2011. Contributions of natural emissions to ozone and PM_{2.5} as
559 simulated by the community multiscale air quality (CMAQ) model. *Environmental*
560 *science & technology* 45, 4817-4823.

561 Natraj, V., Liu, X., Kulawik, S., Chance, K., Chatfield, R., Edwards, D.P., Eldering, A., Francis,
562 G., Kurosu, T., Pickering, K., Spurr, R., Worden, H., 2011. Multi-spectral sensitivity
563 studies for the retrieval of tropospheric and lowermost tropospheric ozone from simulated
564 clear-sky GEO-CAPE measurements. *Atmospheric Environment* 45, 7151-7165.

565 Parrington, M., Jones, D.B.A., Bowman, K.W., Horowitz, L.W., Thompson, A.M., Tarasick,
566 D.W., Witte, J.C., 2008. Estimating the summertime tropospheric ozone distribution over
567 North America through assimilation of observations from the tropospheric emission
568 spectrometer. *Journal of Geophysical Research-Atmospheres* 113, D18307.

569 Reid, N., Yap, D., Bloxam, R., 2008. The potential role of background ozone on current and
570 emerging air issues: An overview. *Air Quality Atmosphere and Health* 1, 19-29.

571 Rodgers, C.D., 2000. *Inverse Methods for Atmospheric Sounding*. World Scientific, River Edge,
572 New Jersey.

573 Selitto, P., Dufour, G., Eremenko, M., Cuesta, J., Foret, G., Gaubert, B., Beekmann, M., Peuch,
574 V.-H., Flaud, J.-M., 2014. Monitoring the lowermost tropospheric ozone with thermal
575 infrared observations from a geostationary platform: performance analyses for a future
576 dedicated instrument. *Atmospheric Measurement Techniques* 7, 391-407.

577 Selitto, P., Del Frate, F., Solimini, D., Casadio, S., 2012. Tropospheric ozone column retrieval
578 from ESA-Envisat SCIAMACHY nadir UV/VIS radiance measurements by means of a
579 neural network algorithm. *IEEE Transactions on Geosciences and Remote Sensing* 50,
580 998-1011.

581 Selitto, P., Di Noia, A., Del Frate, F., Burini, A., Casadio, S., Solimini, D., 2012. On the role of
582 visible radiation in ozone profile retrieval from nadir UV/VIS satellite measurements: An
583 experiment with neural network algorithms inverting SCIAMACHY data. *Journal of*
584 *Quantitative Spectroscopy and Radiative Transfer* 113, 1429-1436.

585 Singh, H.B., Cai, C., Kaduwela, A., Weinheimer, A., Wisthaler, A., 2012. Interactions of fire
586 emissions and urban pollution over California: Ozone formation and air quality
587 simulations. *Atmospheric Environment* 56, 45-51.

588 Timmermans, R.M.A., Segers, A.J., Builtjes, P., Vautard, R., Siddans, R., Elbern, H., Tjemkes,
589 S., Schaap, M., 2009. The added value of a proposed satellite imager for ground level
590 particulate matter analyses and forecasts. *IEEE J. Sel. Top. Appl.*, 2, 271-283.

591 United States Environmental Protection Agency, 2010. Clean air status and trends network
592 second quarter 2010 quality assurance report.

- 593 United States Environmental Protection Agency, 2012. Welfare Risk and Exposure Assessment
594 for Ozone.
- 595 United States Environmental Protection Agency, 2013. Interim Guidance to Implement
596 Requirements for the Treatment of Air Quality Monitoring Data Influenced by
597 Exceptional Events.
- 598 Worden, H.M., Deeter, M.N., Frankenberg, C., George, M., Nichitiu, F., Worden, J., Aben, I.,
599 Bowman, K.W., Clerbaux, C., Coheur, P.F., de Laat, A.T.J., Detweiler, R., Drummond,
600 J.R., Edwards, D.P., Gille, J.C., Hurtmans, D., Luo, M., Martinez-Alonso, S., Massie, S.,
601 Pfister, G., Warner, J.X., 2013. Decadal record of satellite carbon monoxide observations.
602 *Atmospheric Chemistry and Physics* 13, 837-850.
- 603 Yates, E.L., Iraci, L.T., Pierce, R.B., Johnson, M.S., Reddy, P.J., Tadic, J.M., Loewenstein, M.,
604 Gore, W., 2013. Airborne observations and modeling of springtime stratosphere-to-
605 troposphere transport over California. *Atmos. Chem. Phys. Discuss.* 13,
- 606 Zhang, L., Jacob, D.J., Boersma, K.F., Jaffe, D.A., Olson, J.R., Bowman, K.W., Worden, J.R.,
607 Thompson, A.M., Avery, M.A., Cohen, R.C., Dibb, J.E., Flock, F.M., Fuelberg, H.E.,
608 Huey, L.G., McMillan, W.W., Singh, H.B., Weinheimer, A.J., 2008. Transpacific
609 transport of ozone pollution and the effect of recent Asian emission increases on air
610 quality in North America: An integrated analysis using satellite, aircraft, ozonesonde, and
611 surface observations. *Atmospheric Chemistry and Physics* 8, 6117-6136.
- 612 Zhang, L., Jacob, D.J., Liu, X., Logan, J.A., Chance, K., Eldering, A., Bojkov, B.R., 2010.
613 Intercomparison methods for satellite measurements of atmospheric composition:
614 Application to tropospheric ozone from TES and OMI. *Atmospheric Chemistry and*
615 *Physics* 10, 4725-4739.
- 616 Zhang, L., Jacob, D.J., Downey, N.V., Wood, D.A., Blewitt, D., Carouge, C.C., van Donkelaar,
617 A., Jones, D.B.A., Murray, L.T., Wang, Y., 2011. Improved estimate of the policy-
618 relevant background ozone in the United States using the GEOS-chem global model with
619 1/2 degrees x 2/3 degrees horizontal resolution over North America. *Atmospheric*
620 *Environment* 45, 6769-6776.
- 621 Zoogman, P., Jacob, D.J., Chance, K., Worden, H.M., Edwards, D.P., Zhang, L., 2014. Improved
622 monitoring of surface ozone air quality by joint assimilation of geostationary satellite
623 observations of ozone and CO. *Atmospheric Environment* 84, 254-261.
- 624 Zoogman, P., Jacob, D.J., Chance, K., Zhang, L., Le Sager, P., Fiore, A.M., Eldering, A., Liu,
625 X., Natraj, V., Kulawik, S.S., 2011. Ozone air quality measurement requirements for a
626 geostationary satellite mission. *Atmospheric Environment* 45, 7143-7150.